Sensors and Actuators B 191 (2014) 219–226

Contents lists available at ScienceDirect

Sensors and Actuators B: Chemical

journal homepage: www.elsevier.com/locate/snb

Spatially reinforced Au nano-cavities as a reaction nano-reservoir for trace analysis of DNA hybridization

Chih-Kai Yao[a], Jiunn-Der Liao[a,*], Chih-Heng Lin[b], Yuh-Shyong Yang[b], Sheng-Hong Yu[a], Jung-Wei Yang[a]

[a] Department of Materials Science and Engineering, National Cheng Kung University, No. 1, University Road, Tainan 70101, Taiwan
[b] Department of Biological Science and Technology, National Chiao Tung University, 75 Po-Ai Street, Hsinchu 30050, Taiwan

ARTICLE INFO

Article history:
Received 5 August 2013
Received in revised form
12 September 2013
Accepted 30 September 2013
Available online 10 October 2013

Keywords:
Spatially reinforced Au nano-cavities
Nano-reservoir
DNA hybridization
Raman shift
Labeling-free

ABSTRACT

Spatially reinforced Au nano-cavities (*SR-n*Au) with reduced tip-to-tip displacement create strongly localized surface plasmon resonance by Raman scattering. Within *SR-n*Au, the nano-cavity structure with high aspect ratio was optimized as the nano-reservoir for the distinction of DNA hybridization responses from specific DNA sequences of Avian influenza virus. In the nano-reservoir, the suspended or immobilized probe, its complementary and noncomplementary target sequences were characterized at very low concentration through enhanced Raman spectra. The presence of Raman shift at 738 cm^{-1}, the characteristic breathing mode of thymine, and the change of relative peaks intensity at 1603 and 1554 cm^{-1} before and after hybridization were particularly taken as the major indications to validate the match or mismatch state of DNA sequences. Through a labeling-free means, and from the evidence provided by specific complementary and noncomplementary DNA sequences, the recognition capability of nano-reservoir can be down to subnano-molar concentration (10^{-10} M).

1. Introduction

Accurate detection using biomarkers, e.g., antibody, antigen, DNA sequences, at early stages of a disease is of utmost importance in monitoring infectious and contaminated systems [1]. Specific DNA analyses have become a dominant method over the past decade, along with the unraveling genetic codes of variable biomarkers [2,3]. One of the widely established analytical methods is the use of fluorescence spectroscopy [4]; however, some drawbacks mainly correlated with multiplex techniques and stability of fluorescent dyes are presumably resulted. For increasing demands on the fast-screening technologies, e.g., for the control of influenza virus, the development of labeling-free means, where the recognition readouts can be measured directly from the analyze without additional target manipulation, has been constantly emphasized [5]. The related bio-sensing systems may consist of electrical [6,7], fluorescence, surface enhanced Raman scattering (SERS)-based [8,9], and microgravimetric techniques. The technique of SERS has received much attention owing to its high enhancement for directly characterizing the specific molecular bonding of target species. With an appropriate SERS-active substrate, it requires only minimal sample preparation without labeling. In recent years, SERS technique has been increasingly and successfully employed in the study of, e.g., biological molecules [10,11], DNA sequences [12], peptides [13], proteins [14]. Furthermore applications are increasingly applied to, e.g., gene profiling [15], clinical diagnostics [16].

Nano-structure created on a noble metal film with an exceptional SERS property is of great interest for analyzing relatively small size and dimension of target species [17]. As the target species is attached, the effect of SERS may originate from a coupled laser wavelength with dramatic amplification of electromagnetic field accumulated with in the nano-structure, in particular for nano-cavity that may generate a localized surface plasmon resonance (LSPR) [18]. Presumably, the recognition of Raman-active species restricted within the nano-cavity with LSPR will be remarkably enhanced. In addition, comparing nano-rod with nano-cavity structure, the latter has the advantage of capturing target species in solution. Smaller or comparable target species is thus anticipated to be trapped into nano-cavity, then its Raman-active signals can be significantly enhanced by LSPR. In particular, a nano-cavity with multiple edges and a high aspect-ratio angle tend to enhance LSPR [19]. As nano-cavities are uniformly arrayed, the tip-to-tip distance between or among nano-cavities will also influence the

* Corresponding author at: Engineered Materials for Biomedical Applications Group, Department of Materials Science and Engineering, National Cheng Kung University, No. 1, University Road, Tainan 70101, Taiwan. Tel.: +886 6 2757575x62971; fax: +886 6 2003911.
E-mail address: jdliao@mail.ncku.edu.tw (J.-D. Liao).

0925-4005/$ – see front matter © 2013 Elsevier B.V. All rights reserved.
http://dx.doi.org/10.1016/j.snb.2013.09.120

effect of SERS [20]. It has been reported that spatially reinforced Au nano-cavities (*SR-n*Au) with a reduced tip-to-tip displacement are competent to create strong effect of SERS [21]. Based on the electromagnetic theory, a variety of LSPR modes can exist within the nano-cavities of different dimensions, each with its own characteristic electromagnetic field distribution and the resultant effect of SERS [22], which may thereafter provide wide applications in sensing Raman-active species [23].

It is therefore of great interest to apply *SR-n*Au as the nano-reservoir for distincting a controllable reaction of DNA hybridization at an extremely low concentration. For example, DNA sequences can be well distinguished by Raman signals of the labels attached onto its backbone structure [24]. Nevertheless, the obtained signals are those of the labels but not of the oligonucleotide [25]. As a consequence, it is very promising to develop a novel technique to characterize the oligonucleotides directly. DNA hybridization is the most common, specific, and spontaneous reaction between complementary DNA sequences, and it also take an improtant part in most biochemical reaction, followed by polymerase chain reaction (PCR). In this study, target and its complementary DNA sequences under suspension or immobilization condition are anticipated to be annealed and hybridized within the nano-reservoir. To analyze the change from single strands to hybridization responses, annealing temperatures and noncomplementary sequences are taken as the variables and verified. The labeling-free technique for the recognition of DNA hybridization at low concentration is thereafter realized and diagnosed within SERS-active nano-reservoir.

2. Materials and methods

2.1. Fabrication of SERS-active SR-nAu

Au substrate was prepared by thermal evaporation of ≈200 nm of Au (99.99% purity) onto the polished single crystal silicon (1 0 0) wafers (Silicon Sense, Germany) primed with a ≈5 nm-thick titanium adhesion layer. The as-prepared Au substrate surface (shortened as the *ap*Au) was polycrystalline with a grain size of 20–50 nm; its grains predominantly exhibited (1 1 1) orientation. The grain size and the root mean squared roughness (≈0.62 nm) of the *ap*Au were measured by scanning probe microscope (SPA300HV, SEIKO, Japan).

The *SR-n*Au was fabricated using one-step loading-unloading mode of dynamic contact module system (NanoIndenter G200, Agilent Technologies, USA). In the making process, a triangular pyramid tip of *Berkovich* diamond with a radius of ≈20 nm was used under a controlled relative humidity (≈32%) and room temperature (≈24 °C). Before each batch, the nano-indentation tip was cleaned by indenting on the single crystal aluminum. The loading procedure was controlled to have a constant drift rate of 0.05 nm/s for stabilizing the fabrication steps. The applied loading force was in the range of 1500–1700 μN for indentation depths (D_v) of ≈90 nm measured using the vertical displacement. The tip-to-tip displacements (D_{t-t}) of ≈300, ≈500, and ≈700 nm, measured using the parallel displacement, were used. The D_{t-t} and the derived geometrical changes were chosen as the major parameters for comparison.

The field-emission scanning electron microscope (FE-SEM, JSM-7001, JEOL, Japan) was employed to determine the aperture size of cavity (D_a) and D_{t-t}. The measured D_v was referenced in Supplementary data 1. The approaching velocity and the harmonic displacement of the nano-indentation tip toward the target surface were maintained at 1 nm/s and 1 nm for all the testing surfaces. Depending on the unspecified contact points, surface approaching sensitivity was optimized at 10% for the *ap*Au [26].

Table 1
Probe (P) and target (T) sequences of H7 and their modifications.

Name	Description	Sequence 5′–3′
H7-T	H7 target sequence	TACTC-AATTT-GACTG-GGTCA-ATTTG
H7-P	H7 probe sequence	CAAAT-TGACC-CAGTC-AAATT-GAGTA
HS-H7-P	Thiol-terminated H7-P	HS-C6-CAAAT-TGACC-CAGTC-AAATT-GAGTA
Cy3-H7-T	H7-T with Cy3 labeling	Cy3-TACTC-AATTT-GACTG-GGTCA-ATTTG

2.2. Suspended molecular probes and DNA sequences

The *SR-n*Au used for distincting a controllable reaction at an extremely low concentration is called the nano-reservoir. R6G molecule (Sigma, Germany) is commonly used as a tracer dye in biotechnology applications, e.g., the use of fluorescence microscope. It is used as the index to examine the effect of SERS from the target species-included nano-reservoir. R6G solution was diluted with phosphate-buffered saline (PBS, Sigma, Germany) solution to a concentration of 10^{-4} M. Thereafter the nano-reservoir with the molecular probes-containing solution was covered with glass slide and then immediately measured using Raman spectroscopy [27].

All types of DNA sequences used in this study were obtained from MD-Bio Inc. (Taipei, Taiwan), their names and base compositions were shown in Table 1. The target sequence (denoted as H7-T) was a specific biomarker of Avian influenza viruses (AIV), and its complementary sequence (denoted as H7-P) was designed as a capture site for DNA hybridization. These sequences, including the hybridized H7-T/H7-P (denoted as H7-hybrid) were stored at −4 °C before use. Then, they were diluted to 10^{-8}, 10^{-9}, 10^{-10}, and 10^{-11} M in PBS solution for further uses. A quantity of 5 μl from different dilutions of each DNA sequence was placed on the *ap*Au and within the nano-reservoir for subsequent experiments.

2.3. Immobilized DNA sequences on SR-nAu

Alternatively H7-P was immobilized on the nano-reservoir for further bio-sensing applications. At first, the *ap*Au was employed to verify the immobilization process using high resolution X-ray photoelectron spectroscopy (HRXPS, ULVAC Inc., Kanagawa, Japan). The thiol group was modified at the 3′ end of H7-P strand and prepared as the thiol-terminated H7-P (denoted as HS-H7-P), as described in Table 1. This sequence was diluted to 10^{-6} M in PBS solution for further uses. HS-H7-P (10^{-6} M, 10 μl), dithiothreitol (DTT, 0.1 M, 10 μl), and triethylamine (TEA, 0.1 M, 1.5 μl) were mixed to reduce the disulfide bonds at the 5′ end of HS-H7-P and generate free thiol groups for getting immobilization on the *ap*Au and the nano-reservoir at 4 °C for 24 h. After that, the HS-H7-P immobilized surface was washed by deionized water for 10 min, and then stored for further analyses. The HS-H7-P immobilized *ap*Au was labeled with Cyanine dye (Cy3) to verify DNA hybridization. Raman spectra from the HS-H7-P immobilized nano-reservoir were then taken.

2.4. Raman spectroscopy and enhancement factor of SERS

A confocal microscopic Raman spectrometer (In Via Raman microscope, RENISHAW, United Kingdom) using 633 nm radiations from the excitation of He–Ne laser was employed. The excitation power of laser was ≈17 mW and the power on the substrate was ≈8 mW measured by an illumination meter. The scattering light was collected by a 50× air objective lens to a CCD detector. A grating of 1800 lines/mm was used to disperse the scattered light. All the reported Raman spectra were resulted from a single 10 s accumulation in a range of 500–3000 cm^{-1}. Since there was no Raman signal in the range of 2000–3000 cm^{-1}, the spectra in the range of

500–2000 cm^{-1} were presented. Before each batch, Raman shifts were calibrated using the signal of 520 cm^{-1} with the same absolute intensity from a standard silicon wafer.

The enhancement factor (EF) of the measured SERS was estimated according to the standard equation [28]:

$$EF = \frac{I_{SERS}/N_{SERS}}{I_{NRS}/N_{NRS}}, \quad (1)$$

where I_{SERS} and I_{NRS} are SERS and normal Raman scattering intensity, respectively; N_{SERS} and N_{NRS} are the numbers of molecules contributing to the inelastic scattering intensity in each cavity structure, which are respectively evaluated by SERS and normal Raman scattering measurements. The calculated value of EF can represent the ability of inducing SERS effect in each cavity structure. Raman intensity was averaged from ten consecutive measurements. Note that the *ap*Au and the bare nano-reservoir are initially Raman-inactive and used as the reference substrate surface for the calculation of EF when Raman-active R6G molecules are adsorbed within the nano-reservoir.

3. Results and discussion

3.1. Optimization of SR-nAu as the nano-reservoir

FE-SEM photo-images of *SR-n*Au#1, #2, and #3 were presented in Supplementary data 2. The D_a and the aspect ratio, D_v/D_a, of the inter-cavity structure were manipulated by D_{t-t} of each indentation step, the cross-section of cavity structures were observed in Fig. 1. According to the inset figure of Fig. 1, the aspect ratio was correlated with the percentage of volume shrinkage attributed to the mechanically made nano-cavity. For *SR-n*Au#3, each nano-cavity structure was mostly independent; D_a was measured ≈725 ± 8.3 nm. As D_{t-t} was decreased to ≈500 nm (i.e., for *SR-n*Au#2), D_a was 445 ± 8.4 nm. As D_{t-t} was further decreased to ≈300 nm (i.e., for *SR-n*Au#1), D_a was 210 ± 8.3 nm. The nano-cavity structure progressively accumulated and became "spatially reinforced", as D_{t-t} or D_a decreased.

The effect of SERS on *SR-n*Au#1–3 was firstly evaluated using an optimized concentration of 10^{-4} M R6G. In Figure S-2, the major peak of the molecule, designated "P_{R6G}", was clearly found at 1361 cm^{-1} (i.e., assigned to ν(C=C), aromatics). The Raman intensity of "P_{R6G}", denoted as $I_{peak\,(R6G)}$, showed the enhancement. The $I_{peak\,(R6G)}$ values for *SR-n*Au#1–3 increased with the decreasing D_{t-t} or D_a, which were recorded as intensity indicators for subsequent comparisons.

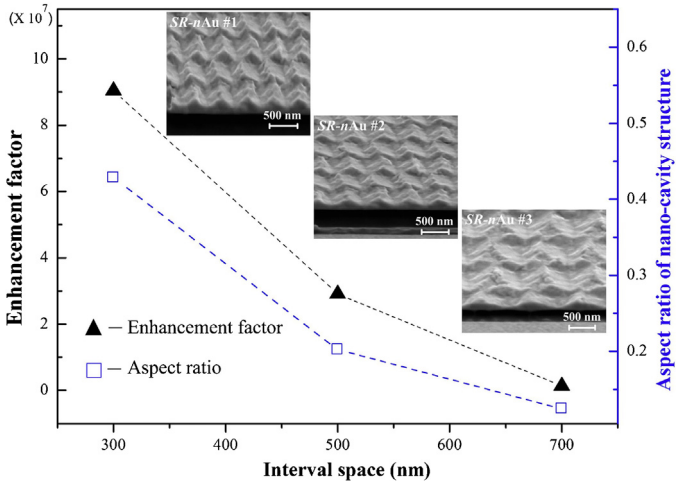

Fig. 1. Raman-active peaks of R6G molecules at 1360 cm^{-1} (P_{R6G}: ν(C=C), aromatics) was taken as the index for the calculation of SERS enhancement factors (▲) and corresponding aspect ratios (●) with respect to their D_{t-t} values within *SR-n*Au#1–3. The insert figures represented the cross-section of nano-cavity structures for *SR-n*Au#1–3.

In Fig. 1, according to Eq. (1), EFs of SERS for *SR-n*Au#1–3 were estimated using $I_{SERS} = I_{peak\,(R6G)}$ and $N_{SERS} = N_{R6G}$. Note that the N_{NRS} value of R6G is estimated using ≈5 μl of 10^{-2} M R6G spread over a diameter of 3 mm, and then the surface is dried off and measured. The average N_{NRS} was calculated ≈4.2×10^9 molecules. The I_{NRS} value was measured ≈150. The I_{SERS} value was divided by the amount of R6G per unit volume to obtain the EF of SERS for one single cavity of *SR-n*Au. In Fig. 1, EFs of SERS decreased with increasing D_{t-t} and decreasing D_a. The optimal EF of SERS for R6G within *SR-n*Au#1 was thereafter estimated ≈9.0×10^7.

R6G molecules were physically adsorbed near *SR-n*Au, $I_{peak\,(R6G)}$ increased with decreasing D_{t-t}. Physically adsorbed R6G molecules within *SR-n*Au#1 were distinguished by a significant enhancement of Raman signals. By comparing the volume of *SR-n*Au, the increase of EF was most probably contributed by LSPs generated within the nano-cavity structure. The *SR-n*Au#1 with a chosen D_{t-t} of ≈300 nm was competent to adjust and maximize the resonance frequency of LSPs and thereafter to induce the electromagnetic effect within the nano-cavity.

3.2. Recognition of single-strand DNA sequences and hybridization

The *SR-n*Au#1 was used as the nano-reservoir for the distinction of DNA hybridization. Based on the dimension of measured area (i.e., 1 μm) by Raman spot, four nano-cavities within *SR-n*Au#1 were defined as one nano-reservoir for the subsequent process of recognizing DNA sequences. In Fig. 2(a), Raman shifts in the range of 600–1800 cm^{-1} appeared as fingerprinting information for H7-T, H7-P, and H7-hybrid, as given in Table 2. Note that H7-T, H7-P, or H7-hybrid on the *ap*Au did not acquire Raman signals. However, as shown in Supplementary data 2, SERS spectra of H7-hybrid within the nano-reservoir over a concentration range of 10^{-8}–10^{-11} M were mostly distinguishable. An optimized detection limit for further studies was preferably chosen at 10^{-10} M, which could be 10–100 times lower than the detection limit of surveyed reports [29].

From Fig. 2(a), (b), and Table 2, Raman shifts in the regions of 650–750 and 1560–1610 cm^{-1} were clearly shown by varying with DNA sequences and annealing temperatures. Raman spectra of H7-P and H7-T showed similar peaks assignment for those at 25 or 95 °C. Relative strong peaks at 1575 (for H7-P) and 1603 cm^{-1} (for H7-T) were respectively distinguished by the arrangement of nucleic acid. In particular, the presence of Raman shift at 738 cm^{-1}, the characteristic breathing mode of thymine, was clearly found for the sequences H7-T (25 and 95 °C), H7-P (25 and 95 °C), and H7-T/H7-P (95 °C) and disappeared for H7-hybrid (25 °C). Relative strong peaks at 1603 (i.e., H7-T, NH_2 (A, G, C)) and 1554 cm^{-1} (i.e., H7-hybrid (25 °C), amide II) were obviously modified after hybridization. In Fig. 2(c), the representing Raman spectra for H7-hybrid (25 °C) and H7-T/H7-P (95 °C) were compared, which indicate DNA hybridization response that changes from double to single-strand by annealing temperatures. In Fig. 2(d), H7-T and H7-P were mixed and annealed within the nano-reservoir from 25 to 95 °C. The values of relative absorbance at 260 nm were recorded, while the hybridization responses were also illustrated. The result corresponded to the presence of Raman shift at 738 cm^{-1}, which indicated the response change from double to single strand by annealing temperatures. Otherwise, the relative intensity of peak at 1554 cm^{-1} showed similar intensity before and after hybridization, because this peak was contributed by amide II from nucleotides. The amount of amide II would not be affected by hybridization,

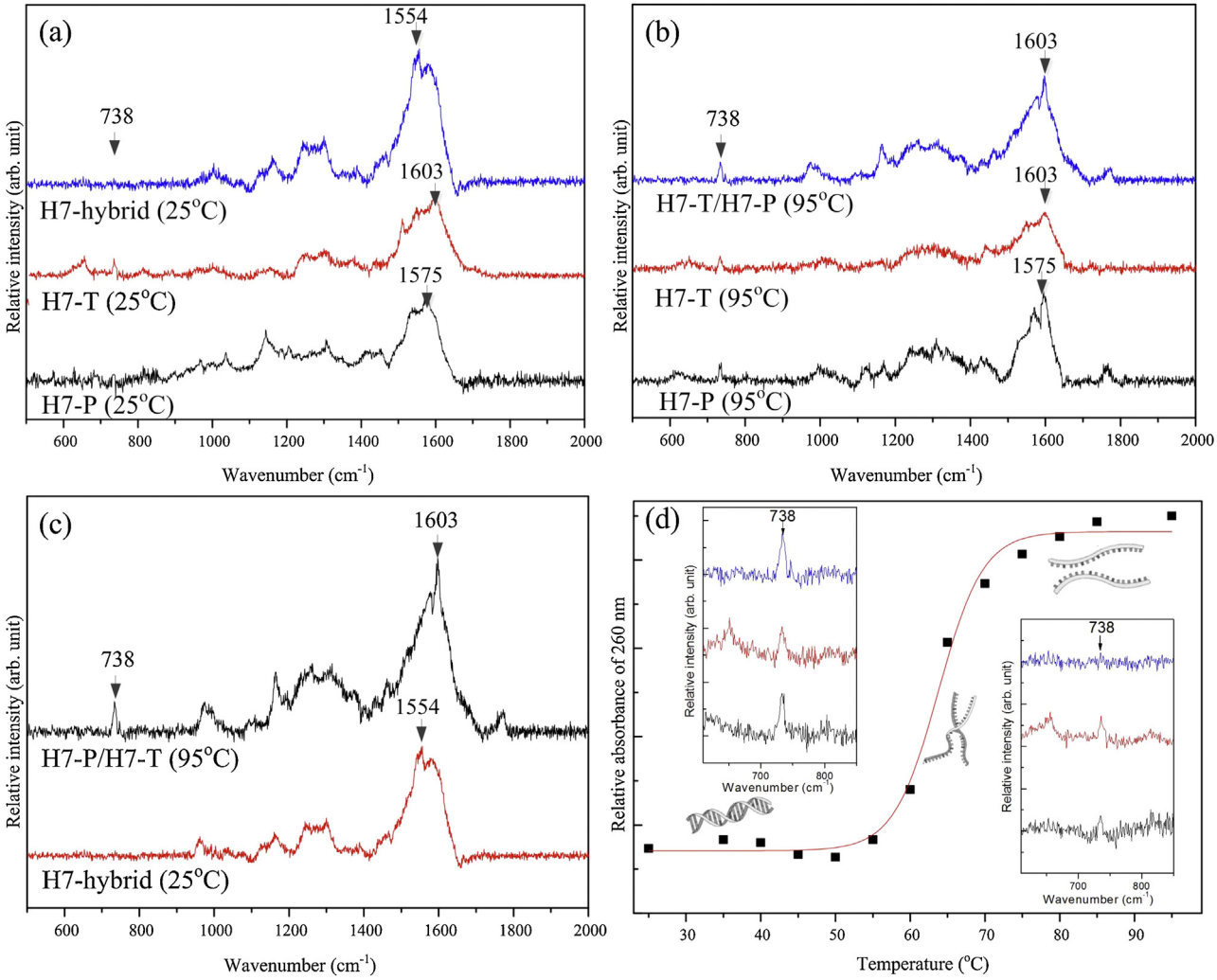

Fig. 2. SERS spectra of target sequence (H7-T), its complementary sequence (H7-P), and hybridized or mixed H7-T/H7-P were measured at different annealing temperatures: (a) 25 °C and (b) 95 °C, respectively. (c) SERS spectra of H7-hybrid (25 °C) and H7-T/H7-P (95 °C) were particularly compared. Raman shifts were assigned and described in Table 2. (d) The mixed H7-T/H7-P was annealed within the nano-reservoir from 25 °C to 95 °C; relative absorbance of 260 nm along with the increase of temperatures was recorded.

Table 2
Raman shifts and assignments for H7-P, H7-T, H7-hybrid (25 °C), and H7-P/H7-T (95 °C).

Raman shift (cm^{-1})	Assignment	H7-P	H7-T	H7-hybrid (25 °C)	H7-T/H7-P (95 °C)
738	Ring breathing mode of T	√	√		√
961	Deoxyribose	√	√	√	√
1181	T, C	√			√
1252	C, A		√	√	√
1306	A	√	√	√	√
1554	Amide II	√	√	√	√
1575	Ring breathing modes G, A	√	√	√	√
1603	NH_2 (A, G, C)	√	√	√	√

so it was taken as a reference for the following comparison. The intensity ratio of 1575 cm^{-1}/1554 cm^{-1} changed from 1.65 to 0.82; this result is reproducible, which indicates that the breathing modes of nucleotides may be changed with the hybridization response. As a result, one may take Raman shift at 738 cm^{-1} as the major indication to validate the match or mismatch state of DNA sequences. The nano-reservoir is therefore competent to identify DNA hybridization responses by identifying Raman shift at 738 cm^{-1} and relative Raman intensity ratio between 1603 and 1554 cm^{-1}.

3.3. Recognition of DNA sequences using H7-P-immobilized nano-reservoir

For practical applications, bio-specimen might contain some impurities, which tended to interfere with, e.g., in this study, the characteristic Raman spectra of H7-T, H7-P, and H7-hybrid sequences. It was therefore preferable to immobilize H7-P upon the nano-reservoir firstly as a capture site, followed by washing away the unbound species. A preliminary study on the HS-H7-P immobilized *ap*Au and then hybridized with H7-T was performed. In

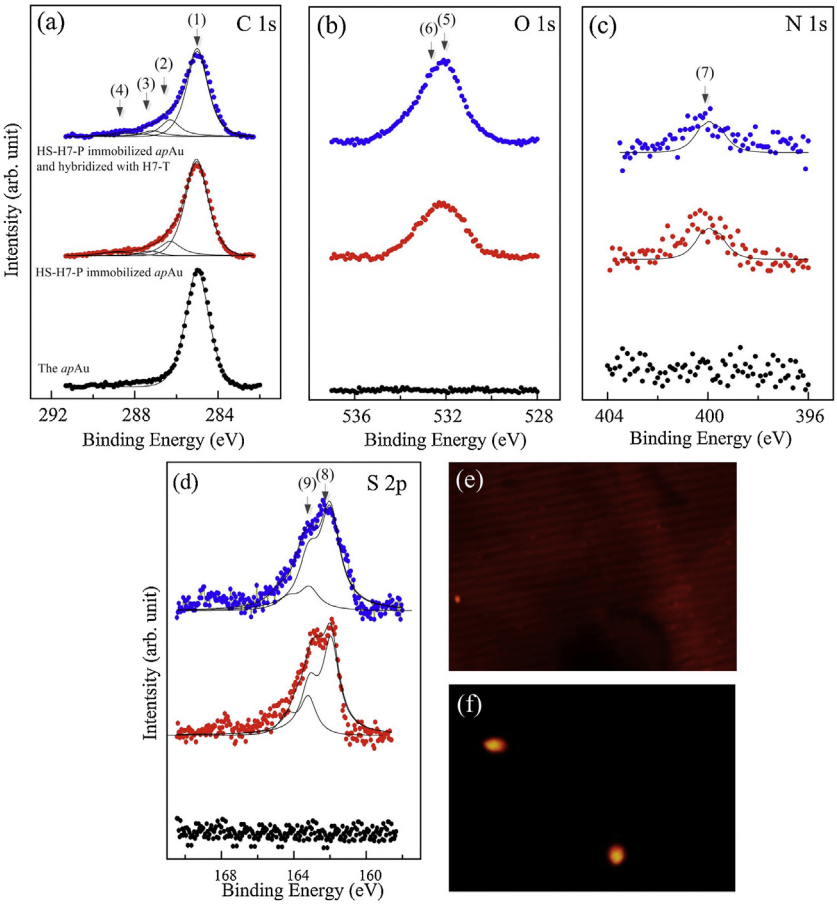

Fig. 3. XPS spectra of (a) C 1s, (b) O 1s, (c) N 1s, and (d) S 2p were presented. To verify the immobilization of HS-H7-P upon the *ap*Au with S-Au bonds, their respective chemical structures with binding energies were given: (1) C—C (285.0 eV), (2) C—O (286.5 eV), (3) C—N (286.7 eV), (4) N—C=O—N (289.0 eV), (5) C=O—N (531.6 eV), (6) C—O—H (532.8 eV), (7) C—N (400.2 eV), (8) S—Au (162.0 eV), and (9) dialkylsufide (163.2 eV). (e) A fluorescent image of Au-S-H7-P/H7-T-Cy3 after washing (in red) was shown. (f) A fluorescent image of suspending H7-P/H7-T-Cy3 after washing (in dark) was also shown. (For interpretation of the references to color in this figure legend, the reader is referred to the web version of the article.)

Fig. 3(a)–(d), C 1s, O 1s, N 1s, and S 2p HRXPS spectra for the respective surfaces were presented. The results indicated that HS-H7-P was firmly immobilized upon the *ap*Au and presumably competent to hybridize with H7-T. The binding energies for peaks (1)–(7) represented the presence of H7-P or H7-hybrid, while those for peaks (8) and (9) showed strong S—Au bond (162.0 eV) on the respective surfaces. In Fig. 3(e) and (f), fluorescent images for the washed Au-S-H7-P/H7-T-Cy3 (in red) and H7-P/H7-T-Cy3 (in dark) were presented. Obviously the washing procedure could remove the unbounded species (e.g., the suspending H7-P/H7-T) from Au surface and remain the immobilized H7-hybrid.

The nano-reservoir was thereafter taken as reaction nano-cavities, in which the suspended H7-hybrid and the immobilized HS-H7-P upon Au, followed by hybridized with H7-T, were studied. The H1-R, which was a mismatch sequence with HS-H7-P, was taken as the reference. Before taking Raman spectra, all the DNA sequences-containing nano-reservoirs were washed. In Fig. 4(a), corresponding to the respective illustrations in Fig. 4(b), Raman shift at 738 cm^{-1} was checked with respect to the suspended H7-hybrid, HS-H7-P/H7-T (25 °C), and HS-H7-P/H1-R (25 °C). For the former two cases, H7-T and H7-P were hybridized and Raman shift at 738 cm^{-1} was disappeared. However, the shift reappeared as the mismatched H1-R sequence was added to HS-H7-P at 25 °C. In addition, the change of major peak intensity from 1554 cm^{-1} (i.e., with hybridization) to 1575 cm^{-1} (i.e., without hybridization, HS-H7-P remained upon Au) could be found as the immobilized HS-H7-P reacted with the respective H7-T and H1-R at 25 °C and then washed. This result indicated that HS-H7-P immobilized nano-reservoir was capable to recognize specific target sequence. It is therefore promising to apply this immobilization method as a labeling-free technique for capturing target sequence and recognizing a specific biomarker correlated with, e.g., a disease.

3.4. *HS-H7-P immobilized nano-reservoir embedded in a micro-fluidic channel*

In Fig. 5(a), FE-SEM micrograph and the layout of the nano-reservoir embedded micro-fluidic channel were presented. In Fig. 5(b), schematic description of a simplified and automated micro-fluidic process was illustrated. Note that the pre-treated bio-specimen is directly transferred from the inlet to the detection area embedded with the nano-reservoir and followed by Raman analysis. After DNA hybridization, PBS solution was entered and washed out the unbounded species.

In Fig. 5(c), R6G molecule was employed to verify the enhancement ability of the micro-fluidic channel. Comparing PDMS with thin glass sheet as the covering materials, relative intensity ratio ($I_{R6G\ (PDMS)}/I_{R6G\ (glass\ sheet)}$) by taking 1361 cm^{-1} (P_{R6G}) as the indication was averaged around 2.54. PDMS was advantageous to be utilized for further application. In Fig. 5(d), typical Raman shifts of HS-H7-P/H7-T (25 °C) and HS-H7-P/H1-R (25 °C) covered with

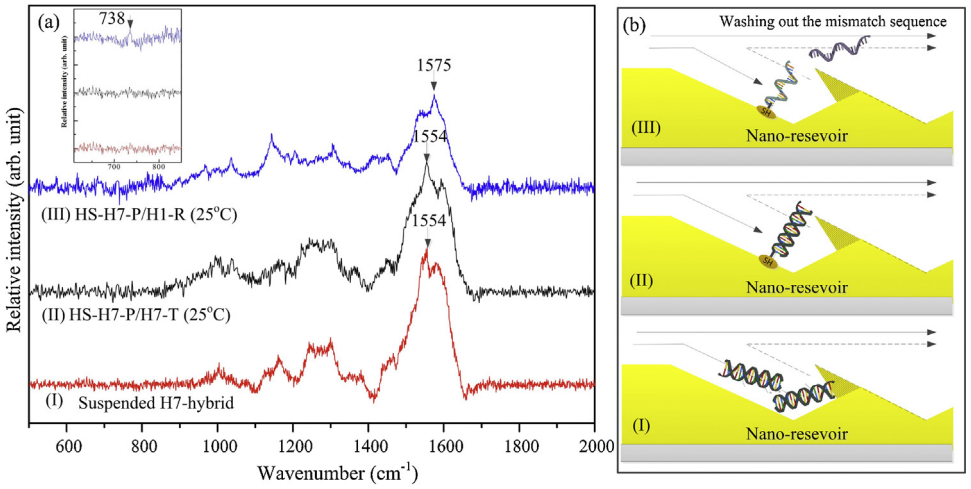

Fig. 4. (a) SERS spectra of H7 sequences with varied mixing reactions within the nano-reservoir, denoted as (I) suspended H7-hybrid, (II) HS-H7-P/H7-T (25 °C), and (III) HS-H7-P/H1-R (25 °C). (b) The corresponding illustrations of mixing reactions (I)–(III) within the nano-reservoir.

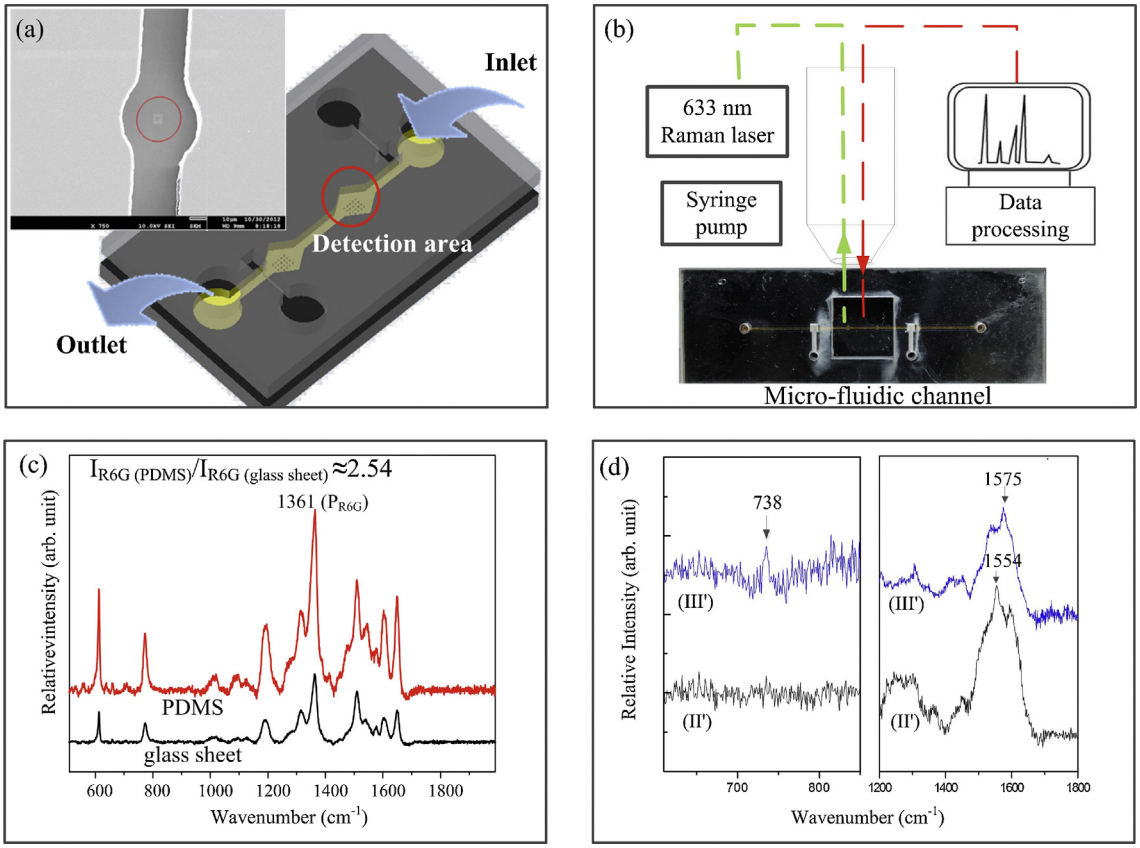

Fig. 5. (a) FE-SEM micrograph of the as-designed nano-reservoir embedded micro-fluidic channel was shown. (b) The nano-reservoir embedded micro-fluidic channel integrated with Raman microscopy as a bio-detection platform was illustrated. (c) Enhancement capabilities of the nano-reservoir embedded micro-fluidic channel covered by glass sheet or PDMS with the same thickness (0.2 mm) were compared. (d) SERS spectra with the major indications of HS-H7-P/H7-T (II′) and HS-H7-P/H1-R (III′) directly analyzed within the nano-reservoir embedded micro-fluidic channel at 25 °C were compared.

PDMS were recorded and denoted as spectra (II′) and (III′). The characteristic spectra were comparable with those in Fig. 4(a), directly analyzed within the nano-reservoir. It is therefore validated that *SR-n*Au#1 is a capable SERS-active substrate to be used as the nano-reservoir for the distinction of specific DNA hybridization into micro-fluidic channel. Furthermore the nano-reservoir immobilized with DNA probe sequence is presumably enabled to be embedded into a micro-fluidic channel for capturing the target DNA sequence without labeling.

4. Conclusion

A novel DNA diagnostic method based on the reaction nano-reservoir has been developed. In this study, *SR-n*Au with high

aspect ratio for the nano-reservoir was firstly optimized using R6G molecule as the probe and the EF of SERS was estimated ≈9.0×10^7. Specific biomarkers of AIV, H7-T, H7-P, and H7-hybrid, within the nano-reservoir over a concentration range of 10^{-8}–10^{-11} M were mostly distinguishable. Raman shifts for the presence of 738 cm^{-1} and relative intensities among 554, 1575, and 1603 cm^{-1} were used as the major indications to validate the match or mismatch state of DNA sequences at 25 and 95 °C. Thereafter the HS-H7-P immobilized nano-reservoir, in comparison with the suspended H7-hybrid, was taken as the reaction nano-cavities, hybridized with H7-T and H1-R (a mismatch sequence with HS-H7-P) at 25 °C, and then washed. Raman shifts for the presence of 738 cm^{-1} and the change of major peak intensity from 1554 (i.e., with hybridization) to 1575 cm^{-1} (i.e., without hybridization, HS-H7-P remained upon Au) could be clearly found. Furthermore HS-H7-P immobilized nano-reservoir was embedded into a microfluidic channel and covered with PDMS; the integrated system was competent to capture and distinguish the target DNA sequence. Through labeling-free means, the recognition capability of SERS-active nano-reservoir for DNA sequences could be down to 10^{-10} M.

Acknowledgements

This work was financially supported by National Science Council of Taiwan under Grant No. NSC-100-2221-E-006-025-MY3 and Medical Device Innovation Center of National Cheng Kung University under the Grant No. D102-21007, and Headquarters of University Advancement, NCKU, under the Grant No. D102-33B08.

Appendix A. Supplementary data

Supplementary data associated with this article can be found, in the online version, at http://dx.doi.org/10.1016/j.snb.2013.09.120.

References

[1] Y. Wang, X. Hu, J.A. Wang, M. Xiang, J. Yu, F. Liu, Application of serum protein fingerprint in diagnosis of coronary artery disease, Clinical Biochemistry 44 (2011) 185–191.
[2] C.A. Harrington, C. Rosenow, J. Retief, Monitoring gene expression using DNA microarrays, Current Opinion in Microbiology 3 (2000) 285–291.
[3] D.J. Lockhart, E.A. Winzeler, Genomics, gene expression and DNA arrays, Nature 405 (2000) 827.
[4] K.K. Strelau, R. Kretschmer, R. Möller, W. Fritzsche, J. Popp, SERS as tool for the analysis of DNA-chips in a microfluidic platform, Analytical & Bioanalytical Chemistry 396 (2010) 1381–1384.
[5] H.I. Peng, C.M. Strohsahl, K.E. Leach, T.D. Krauss, B.L. Miller, Label-free DNA detection on nanostructured Ag surfaces, ACS Nano 3 (2009) 2265–2273.
[6] C. Fan, K.W. Plaxco, A.J. Heeger, Electrochemical interrogation of conformational changes as a reagentless method for the sequence-specific detection of DNA, Proceedings of the National Academy of Sciences of the United States of America 100 (2003) 9134–9137.
[7] A. Erdem, M.I. Pividori, A. Lermo, A. Bonanni, M.D. Valle, S. Alegret, Genomagnetic assay based on label-free electrochemical detection using magneto-composite electrodes, Sensors and Actuators B: Chemical 114 (2006) 591–598.
[8] I. Mannelli, M. Minunni, S. Tombelli, R. Wang, M. Michela Spiriti, M. Mascini, Direct immobilisation of DNA probes for the development of affinity biosensors, Bioelectrochemistry 66 (2005) 129–138.
[9] X. Yao, X. Li, F. Toledo, C. Zurita-Lopez, M. Gutova, J. Momand, et al., Sub-attomole oligonucleotide and p53 cDNA determinations via a high-resolution surface plasmon resonance combined with oligonucleotide-capped gold nanoparticle signal amplification, Analytical Biochemistry 354 (2006) 220–228.
[10] L. Lu, K. Ai, Y. Ozaki, Environmentally friendly synthesis of highly monodisperse biocompatible gold nanoparticles with urchin-like shape, Langmuir 24 (2008) 1058–1063.
[11] S.C. Pînzaru, L.M. Andronie, I. Domsa, O. Cozar, S. Astilean, Bridging biomolecules with nanoparticles: surface-enhanced Raman scattering from colon carcinoma and normal tissue, Journal of Raman Spectroscopy 39 (2008) 331–334.
[12] W. Ke, D. Zhou, J. Wu, K. Ji, Surface-enhanced Raman spectra of calf thymus DNA adsorbed on concentrated silver colloid, Applied Spectroscopy 59 (2005) 418–423.
[13] C. Bernal, E. Mendez, J. Terencio, A. Boronat, S. Imperial, A spectrophotometric assay for the determination of 4-diphosphocytidyl-2-C-methyl-D-erythritol kinase activity, Analytical Biochemistry 340 (2005) 245–251.
[14] X. Huang, I.H. El-Sayed, W. Qian, M.A. El-Sayed, Cancer cell imaging and photothermal therapy in the near-infrared region by using gold nanorods, Journal of the American Chemical Society 128 (2006) 2115–2120.
[15] Y. Chen, G. Chen, S. Feng, J. Pan, X. Zheng, Y. Su, et al., Label-free serum ribonucleic acid analysis for colorectal cancer detection by surface-enhanced Raman spectroscopy and multivariate analysis, Journal of Biomedical Optics 17 (2012) 067003.
[16] L. Bi, Y. Rao, Q. Tao, J. Dong, T. Su, F. Liu, et al., Fabrication of large-scale gold nanoplate films as highly active SERS substrates for label-free DNA detection, Biosensors and Bioelectronics 43 (2013) 193–199.
[17] X.Y. Zhang, A. Hu, T. Zhang, W. Lei, X.J. Xue, Y. Zhou, et al., Self-assembly of large-scale and ultrathin silver nanoplate films with tunable plasmon resonance properties, ACS Nano 5 (2011) 9082–9092.
[18] P.J. Schuck, D.P. Fromm, A. Sundaramurthy, G.S. Kino, W.E. Moerner, Improving the mismatch between light and nanoscale objects with gold bowtie nanoantennas, Physical Review Letters 94 (2005) 017402.
[19] N. Perney, J. Baumberg, M. Zoorob, M. Charlton, S. Mahnkopf, C. Netti, Tuning localized plasmons in nanostructured substrates for surface-enhanced Raman scattering, Optics Express 14 (2006) 847–857.
[20] Z. Zhu, H. Meng, W. Liu, X. Liu, J. Gong, X. Qiu, et al., Superstructures and SERS properties of gold nanocrystals with different shapes, Angewandte Chemie International Edition 50 (2011) 1593–1596.
[21] C.K. Yao, J.D. Liao, C.W. Chang, J.R. Lin, Spatially reinforced nano-cavity array as the SERS-active substrate for detecting hepatitis virus core antigen at low concentrations, Sensors and Actuators B: Chemical 174 (2012) 478–484.
[22] M.D. Charlton, C.M. Netti, M. Zoorob, N. Perney, J. Baumberg, Organising light on the nano-scale: surface plasmon engineering for repeatable SERS sensing and applications for trace analyte detection, ECS Transactions 3 (2006) 79–89.
[23] C.W. Chang, J.D. Liao, A.L. Shiau, C.K. Yao, Non-labeled virus detection using inverted triangular Au nano-cavities arrayed as SERS-active substrate, Sensors and Actuators B: Chemical 156 (2011) 471–478.
[24] C. Fang, A. Agarwal, K.D. Buddharaju, N.M. Khalid, S.M. Salim, E. Widjaja, et al., DNA detection using nanostructured SERS substrates with Rhodamine B as Raman label, Biosensors and Bioelectronics 24 (2008) 216–221.
[25] L. Sun, Y. Song, L. Wang, C. Guo, Y. Sun, Z. Liu, et al., Ethanol-induced formation of silver nanoparticle aggregates for highly active SERS substrates and application in DNA detection, The Journal of Physical Chemistry C 112 (2008) 1415–1422.
[26] Y.T. Yang, J.D. Liao, Y.L. Lee, C.W. Chang, T.H. Jung, Ultra-thin phospholipid layers physically adsorbed upon glass characterized by nano-indentation at the surface contact level, Nanotechnology 20 (2009) 195702.
[27] C.W. Chang, J.D. Liao, Y.Y. Lin, C.C. Weng, Detecting very small quantity of molecular probes in solution using nano-mechanically made Au-cavities array with SERS-active effect, Sensors and Actuators B: Chemical 153 (2011) 271–276.
[28] K.L. Wustholz, C.L. Brosseau, F. Casadio, R.P. Van Duyne, Surface-enhanced Raman spectroscopy of dyes: from single molecules to the artists' canvas, Physical Chemistry Chemical Physics 11 (2009) 7350–7359.
[29] J.D. Driskell, R.A. Tripp, Label-free SERS detection of microRNA based on affinity for an unmodified silver nanorod array substrate, Chemical Communications 46 (2010) 3298–3300.

Biographies

Chih-Kai Yao is currently pursuing his Ph.D. degree in materials science and engineering from National Cheng-Kung University (NCKU), Tainan, Taiwan. He received his B.S. and M.S. degrees in material science and engineering from NCKU in 2007 and 2009, respectively. His current research interests are focused on the fabrication of SERS-active substrate for fast-screening detection platform using the nano-indentation technique.

Jiunn-Der Liao is currently a professor at the Department of Materials Science & Engineering, NCKU, Tainan, Taiwan. He obtained his B.S. degree at NCKU (1984), M.S. degree at K.U. Leuven (1990 and 1991) in Belgium, and Ph.D. degree at ENS Mines (1994) in France. He also worked at the University of Heidelberg (1995–1996) in Germany and Chung Yuan Christian University (1996–2002) in Taiwan. His current research interests are focused upon (1) mechanics of biomaterials, e.g., tissue engineering, scaffold materials, cell-surface interactions, nano-indentation, mechanical transduction; (2) plasma chemistry and plasma processing, e.g., plasma generation, plasma diagnoses, plasma physics and chemistry, metal vapor vacuum arc, plasma ion immersion; and (3) nano-fabrication and nano-characterization, e.g., focused ion beam based nano-fabrication, micro-contact imprinting, synchrotron-based and laboratory-based high resolution analyses.

Chih-Heng Lin obtained his Ph.D. degree at biological science and engineering, in NCTU, Hsinchu, Taiwan. The research topic of his Ph.D. degree was focused on the poly-silicon nanowire field-effect transistor for ultrasensitive and label-free detection of pathogenic avian influenza DNA.

Yuh-Shyong Yang is currently a professor at the Department of Biological Science and Engineering, NCTU, Hsinchu, Taiwan. He obtained his Ph.D. degree with the major in Biochemistry in University of Wisconsin-Madison. His current research

interests are focused upon: enzyme and protein, engineering, proteomics, enzyme, mechanisms of enzyme action and protein engineering, bioelectronics and enzyme chip.

Sheng-Hong Yu obtained his B.S. and M.S. degrees in materials science and engineering from NCKU in 20011 and 2013, respectively. The research topic of his Master degree was focused on the fabrication of SERS-active substrate for fast-screening detection platform using the nano-indentation technique.

Jung-Wei Yang obtained his B.S. degrees in materials science and engineering from NCKU in 2013. The research topic of his Bachelor degree was focused on applying SERS-active substrate for fast-screening detection.